RTA-408 induces JNK-dependent apoptosis and autophagy in breast cancer cells

YU-JEN CHEN[1], HUNG-PEI TSAI[2], MEI-YIN CHEN[3], I-HSIANG CHEN[4], WEI-CHIEH CHEN[4], TZU-TING TSENG[2], CHEN-YU WANG[5] and JIA-HAU LEE[6]

[1]Department of Gynecologic Oncology, An-Nan Hospital, China Medical University, Tainan 709, Taiwan, R.O.C.; [2]Division of Neurosurgery, Department of Surgery, Kaohsiung Medical University Hospital, Kaohsiung Medical University, Kaohsiung 807, Taiwan, R.O.C.; [3]Department of Laboratory Medicine, Kaohsiung Medical University Hospital, Kaohsiung 807, Taiwan, R.O.C.; [4]Department of Pathology, Kaohsiung Medical University Hospital, Kaohsiung Medical University, Kaohsiung 807, Taiwan, R.O.C.; [5]Department of Radiation Oncology, Kaohsiung Medical University Hospital, Kaohsiung Medical University, Kaohsiung 807, Taiwan, R.O.C.; [6]Department of Clinical Research, An-Nan Hospital, China Medical University, Tainan 709, Taiwan, R.O.C.

Received December 12, 2025; Accepted April 22, 2026

DOI: 10.3892/ol.2026.15692

Abstract. RTA-408 is a synthetic activator of the nuclear factor erythroid 2-related factor 2 pathway with antioxidant and anti-inflammatory act2ivity, but its antitumor effects in breast cancer (BC) have not fully been defined. The present study evaluated the antiproliferative efficacy and underlying mechanisms of RTA-408 in BC cells. Estrogen receptor-positive MCF-7 and triple-negative MDA-MB-231 BC cells were exposed to 0-1,000 nM RTA-408 for 72 h in standard serum-containing culture medium. Cell viability was quantified using a tetrazolium-based colorimetric assay and apoptosis was evaluated by the Muse® Annexin V & Dead Cell assay based on Annexin V and 7-amino-actinomycin D staining; the expression levels of JNK, p38, ERK, beclin-1, microtubule-associated protein 1 light chain 3B (LC3B), p62/sequestosome 1 (SQSTM1) and poly (ADP-ribose) polymerase (PARP) were assessed by western blotting. Pathway dependence was examined using the JNK inhibitor SP600125. Results showed that RTA-408 reduced cell viability in a concentration-dependent manner, with an IC_{50} of ~400 nM, decreasing survival to 28% in MCF-7 cells and 22% in MDA-MB-231 cells at 1,000 nM. RTA-408 increased annexin V^+ apoptotic fractions, enhanced PARP cleavage and increased beclin-1, LC3B and p62/SQSTM1 levels. RTA-408 markedly enhanced JNK phosphorylation, with more modest activation of p38 and ERK. Pharmacological inhibition with SP600125 attenuated JNK phosphorylation, reduced apoptotic responses and diminished autophagy-associated marker accumulation, supporting the notion that JNK signaling contributes, at least in part, to these effects. These findings indicate that RTA-408 exerts nanomolar antiproliferative activity in both hormone receptor-positive and triple-negative BC cells through a JNK-dependent mechanism that simultaneously engages apoptosis and autophagy, supporting further *in vivo* and translational investigation.

Correspondence to: Dr Jia-Hau Lee, Department of Clinical Research, An-Nan Hospital, China Medical University, 66 Sector 2, Changhe Road, Tainan 709, Taiwan, R.O.C.
E-mail: 170252@tool.caaumed.org.tw

Key words: RTA-408, JNK, apoptosis, autophagy, breast cancer

Introduction

Breast cancer (BC) remains the most commonly diagnosed cancer among women worldwide. According to the most recent GLOBOCAN 2022 estimates from the International Agency for Research on Cancer, BC accounted for 2,296,840 new cases and 666,103 deaths worldwide in 2022 (1). Notably, the global BC incidence is expected to increase by >40% by 2040 (2), with China exhibiting the highest incidence rate in Asia (3). BC is a heterogeneous disease that is classified by the expression of key receptors, such as the estrogen receptor (ER), progesterone receptor (PR) and HER2 (4). Furthermore, ~75% of BC cases are ER^- and/or PR^+ (5), making adjuvant endocrine therapy (AET) a standard treatment that notably reduces recurrence and mortality and improves overall survival (6-8). The American Society of Clinical Oncology recommends 5-10 years of AET (9); however, its prolonged use is often associated with adverse effects, including hot flashes, night sweats, fatigue, sleep disturbance, sexual dysfunction, joint stiffness, joint dysfunction and joint pain, all of which may adversely affect patients' quality of life (10). In addition, 15-25% of BC cases are characterized by HER2 overexpression or gene amplification (11,12), which is associated with more aggressive disease, higher histological grade, early metastasis and worse prognosis (12-14).

RTA-408 (omaveloxolone) is a synthetic oleanane triterpenoid with broad biological activity owing to its ability to modulate redox-sensitive transcriptional pathways. It

binds to kelch-like ECH-associated protein 1 (KEAP1) at a critical cysteine residue, thereby stabilizing nuclear factor erythroid 2-related factor 2 (Nrf2) and inducing the expression of antioxidant and phase II detoxification genes, including sulfiredoxin, thioredoxin, thioredoxin reductase, glutathione reductase, peroxiredoxin, glutamate cysteine ligase and quinone reductase (15). Nrf2 activation bolsters cellular antioxidant defenses and exerts anti-inflammatory effects by attenuating reactive oxygen species-driven inflammatory signaling (15). RTA-408 also inhibits IKK, blocking NF-κB activation and consequently reducing pro-inflammatory gene expression while promoting apoptosis in cancer cells (15). In addition, it affects the heme-regulated transcriptional repressor BTB and CNC homolog 1 (BACH1); in models of acute lung injury, RTA-408 prevents ferroptotic cell death by suppressing BACH1 activity (16). These mechanisms translate into cytoprotective outcomes in diverse preclinical models. RTA-408 mitigates oxidative tissue damage and inflammation and inhibits tumor growth in xenograft cancer models (15). Clinically, a first-in-human phase I trial in patients with stage IV relapsed/refractory melanoma or non-small cell lung cancer showed that oral RTA-408 was well tolerated at biologically active doses (with evidence of Nrf2 target engagement and minimal toxicity), although no confirmed tumor responses were observed (15). In a pivotal placebo-controlled trial for Friedreich's ataxia (a neurodegenerative disease), omaveloxolone treatment improved neurological function compared with placebo, as demonstrated by a 2.40±0.96-point placebo-corrected improvement in modified Friedreich's Ataxia Rating Scale (mFARS) score at week 48, with improvements observed across mFARS components, including bulbar function, upper-limb coordination, lower-limb coordination and upright stability, most notably upright stability (17). This benefit, along with a manageable safety profile, has resulted in the approval of omaveloxolone as the first-line therapy for Friedreich's ataxia (18). Ongoing research is exploring the therapeutic potential of omaveloxolone in other conditions, such as inflammatory bowel disease, by leveraging its antioxidant, anti-inflammatory and immunomodulatory properties (18). The efficacy of omaveloxolone in BC remains unexplored; therefore, the present study aimed to investigate the antitumor efficacy and underlying mechanisms of RTA-408 in BC.

Materials and methods

Cell culture. Human BC cell lines, MCF-7 (ER^+) and MDA-MB-231 (triple-negative), were obtained from the Bioresource Collection and Research Center. MCF-7 cells were cultured in RPMI-1640 (cat. no. 31800-022; Gibco; Thermo Fisher Scientific, Inc.), whereas MDA-MB-231 cells were cultured in DMEM (cat. no. 31600-034; Gibco; Thermo Fisher Scientific, Inc.). The culture medium included 10% heat-inactivated FBS (cat. no. FC926; MilliporeSigma; Merck KGaA), 100 U/ml penicillin and 100 μg/ml streptomycin at 37˚C in a humidified 5% CO_2 incubator. Cultures were passaged 2-3 times per week and used within 20 passages.

Drug preparation and treatment. RTA-408 (cat. no. HY-12212; MedChemExpress) and SP600125 (cat. no. HY-12041; MedChemExpress) were dissolved in DMSO to prepare 10 mM stock solutions and stored at -20˚C. Working solutions were freshly prepared in complete medium; the final DMSO concentration did not exceed 0.1%. For JNK blockade, cells were pre-incubated for 1 h at 37˚C with 10 μM SP600125 before the addition of RTA-408. Vehicle controls received an equivalent volume of DMSO.

Cell-viability assay. Exponentially growing cells were seeded in 24-well plates at a density of $3x10^4$ cells/well. After overnight attachment, the cultures were exposed to RTA-408 at 0-1,000 nM for 72 h at 37˚C. Viability was quantified using an MTT assay (cat. no. L11939.06; Thermo Fisher Scientific, Inc.) according to the manufacturer's instructions. Formazan crystals were dissolved in 200 μl DMSO, and absorbance was read at 570 nm on an ELISA reader (MULTISKAN FC; Thermo Fisher Scientific, Inc.). The results are expressed as a percentage of the untreated control. Each condition was performed in triplicate in six independent experiments.

Apoptosis flow cytometry. Apoptosis was analyzed using a Muse® Annexin V & Dead Cell Kit (cat. no. MCH100105; Cytek Biosciences) according to the manufacturer's instructions. After treatment, $3x10^5$ cells were collected, washed twice with PBS and resuspended in 100 μl of the staining reagent supplied with the Kit. Following a 15 min incubation (room temperature, in the dark), samples were diluted to 500 μl and immediately analyzed on a flow cytometer (MUSE; Cytek Biosciences). For each sample, 20,000 events were recorded.

Western blotting. Cells were lysed in RIPA buffer supplemented with protease (cat. no. 04693159001; Roche Diagnostics GmbH) and phosphatase inhibitors (cat. no. 04906845001; Roche Diagnostics GmbH). Equal amounts of protein (50 μg) were separated by 10-12% SDS-PAGE gel electrophoresis and electro-transferred to PVDF membranes (cat. no. NEF1002001PK; PerkinElmer, Inc.). After blocking with 5% non-fat milk for 1 h at room temperature, membranes were incubated overnight at 4˚C with primary antibodies against phosphorylated-JNK (p-JNK; 1:500; cat. no. 4668; Cell Signaling Technology, Inc.), total JNK (1:1,000; cat. no. 9252; Cell Signaling, phosphorylated-p38 (p-p38; 1:500; cat. no 9211; Cell Signaling Technology, Inc.), total p38 (1:1,000; cat. no. 9212; Cell Signaling Technology, Inc.), phosphorylated ERK1/2 (p-ERK1/2; 1:500; cat. no. 9101; Cell Signaling Technology, Inc.), total ERK1/2 (1:2,000; cat. no. 9102; Cell Signaling Technology, Inc.), beclin-1 (1:1,000; cat. no. 11306-1-AP; Proteintech Group, Inc.), light-chain 3B (LC3B; 1:1,000; cat. no. 3868; Cell Signaling Technology, Inc.), p62 (1:1,000; cat. no. 18420-1-AP; Proteintech Group, Inc.), poly(ADP-ribose) polymerase (PARP; 1:1,000; cat. no. 13371-1-AP; Proteintech Group, Inc.) and β-actin (1:20,000; cat. no. A5441; MilliporeSigma). HRP-conjugated secondary antibodies (goat anti-rabbit antibody: cat. no. AP132P; 1:5,000; MilliporeSigma; and goat anti-mouse antibody: cat. no. AP124P; 1:5,000; MilliporeSigma; Merck KGaA) were applied for 1 h at room temperature and signals were visualized using Western Lightning™ Plus-ECL substrate (Revvity, Inc.) on a ChemiDoc MP imaging system (8.0.2.0/21; Wuhan Servicebio Technology Co., Ltd.). Band

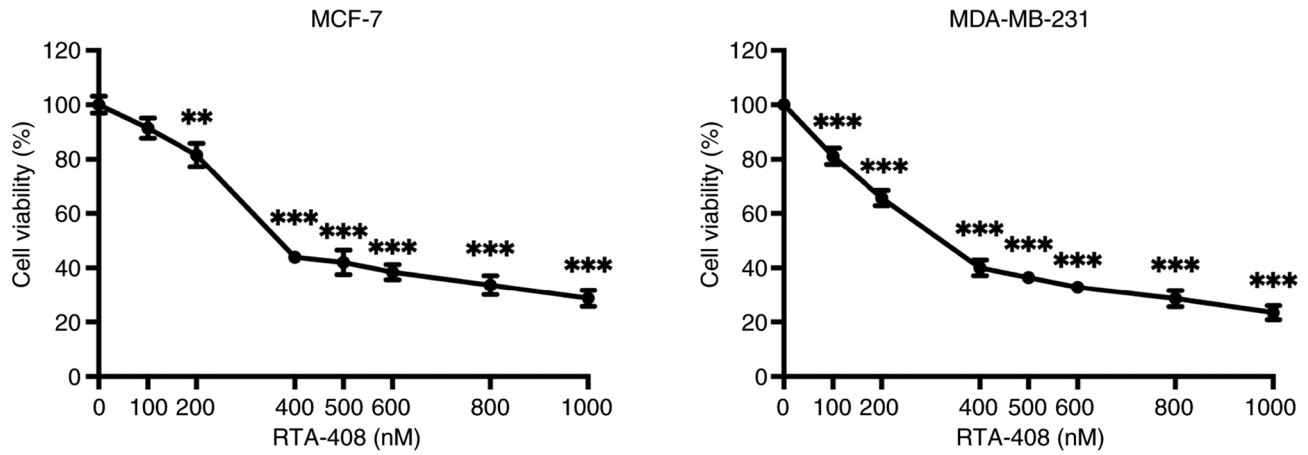

Figure 1. Dose-dependent reduction of cell viability following 72 h RTA-408 exposure. MCF-7 and MDA-MB-231 cells were treated with vehicle (0.1% DMSO) or RTA-408 (omaveloxolone) at the indicated concentrations (0-1,000 nM) for 72 h. Cell viability was quantified by MTT and normalized to the vehicle control (set to 100%). Data are presented as the mean ± SD (n=6). Solid circles denote means and error bars indicate SD. Statistical significance was assessed by one-way ANOVA, followed by Tukey's post hoc test. **P<0.01 and ***P<0.001 vs. the control.

intensities were quantified using ImageJ ('Fiji' package; version 2.9.0; National Institutes of Health) and normalized to β-actin.

Statistical analysis. Data are presented as the mean ± SD from ≥6 independent experiments. Statistical significance was assessed using one-way ANOVA, followed by Tukey's post hoc test (GraphPad Prism; version 9; Dotmatics). P<0.05 was considered to indicate a statistically significant difference, with *P<0.05, **P<0.01 and ***P<0.001 vs. the control and $^{\#}$P<0.05 and $^{\#\#}$P<0.01 vs. the corresponding RTA-408 group.

Results

Dose-dependent reduction of cell viability in MCF-7 and MDA-MB-231 BC cells following RTA-408 treatment. To assess concentration-dependent cytotoxicity, MCF-7 BC cells were exposed to 0-1,000 nM RTA-408 for 72 h, after which cell viability was quantified using an MTT assay (Fig. 1). Cell survival remained close to baseline at 100 nM and decreased to 81.52±12.40% at 200 nM (P<0.01 vs. control). A sharper decline was observed at 400 nM, where viability decreased to 43.93±6.18% and further reductions were recorded between 500-600 nM (42.08±13.49% and 38.41±8.54%, respectively), with all values from 400 nM onward achieving P<0.001. At the highest doses of 800 and 1,000 nM, viability decreased by 33.61±10.51% and 28.74±8.95%, respectively (P<0.001).

Under identical treatment conditions, MDA-MB-231 cells exhibited a monotonic loss of viability (Fig. 1). Viability remained near 80% at 100 nM (P<0.001), followed by a reduction to 65.65±8.39% survival at 200 nM (P<0.001). Exposure to 400 nM lowered viability to 40.0±8.40%, with a gradual decline to 36.48±6.34% and 28.64±8.59% at 600 and 800 nM, respectively (P<0.001). The maximal concentration of 1,000 nM reduced viability to 23.42±7.90% (P<0.001). These data demonstrate that RTA-408 induced a robust, dose-dependent cytotoxic response in both HR^{+} and triple-negative BC cell models, supporting its potential as a broadly effective antiproliferative agent.

Dose-dependent induction of apoptosis and autophagy by RTA-408 in BC cells. Quantification of Annexin V-positive cells revealed a dose-dependent increase in total apoptosis after 72 h of RTA-408 treatment in both MCF-7 and MDA-MB-231 cells (Fig. 2A). In MCF-7 cells, the apoptotic fraction increased progressively with increasing drug concentration and reached statistical significance at 400 nM (P<0.001), whereas the increases at 100 and 200 nM did not reach statistical significance. In MDA-MB-231 cells, RTA-408 also produced a clear dose-dependent increase in apoptosis, with significant elevations observed at 100 and 200 nM (both P<0.01) and at 400 nM (P<0.001).

PARP cleavage was additionally examined by western blotting as a biochemical indicator of apoptosis. A lower band consistent with cleaved PARP was detectable, particularly at higher RTA-408 concentrations; however, the cleaved PARP signal was relatively weak compared with the robust increase in Annexin V-positive apoptotic fractions observed by flow cytometry (Fig. 2B). Therefore, PARP cleavage was interpreted as complementary biochemical evidence, whereas flow cytometry served as the primary quantitative assessment of apoptosis.

Western blotting analysis was further used to examine the autophagy-related markers Beclin-1, LC3B-II and p62 (Fig. 2B). In MCF-7 cells, Beclin-1 showed a moderate increase after RTA-408 treatment, although this increase did not reach statistical significance. LC3B-II was significantly increased at 200 nM (P<0.001) and 400 nM (P<0.05), whereas p62 was significantly elevated at 100, 200 and 400 nM (all P<0.01). In MDA-MB-231 cells, Beclin-1 reached statistical significance at 100 nM (P<0.05), while the increases at 200 and 400 nM did not reach statistical significance. LC3B-II was significantly increased at 200 and 400 nM (both P<0.05) and p62 reached statistical significance at 400 nM (P<0.05). Collectively, these findings indicate that RTA-408 induces apoptosis and is accompanied by accumulation of autophagy-related markers in breast cancer cells.

Dose-dependent activation of MAPK signaling cascades by RTA-408 in BC cells. To elucidate whether RTA-408 modulates stress-activated MAPK signaling, the

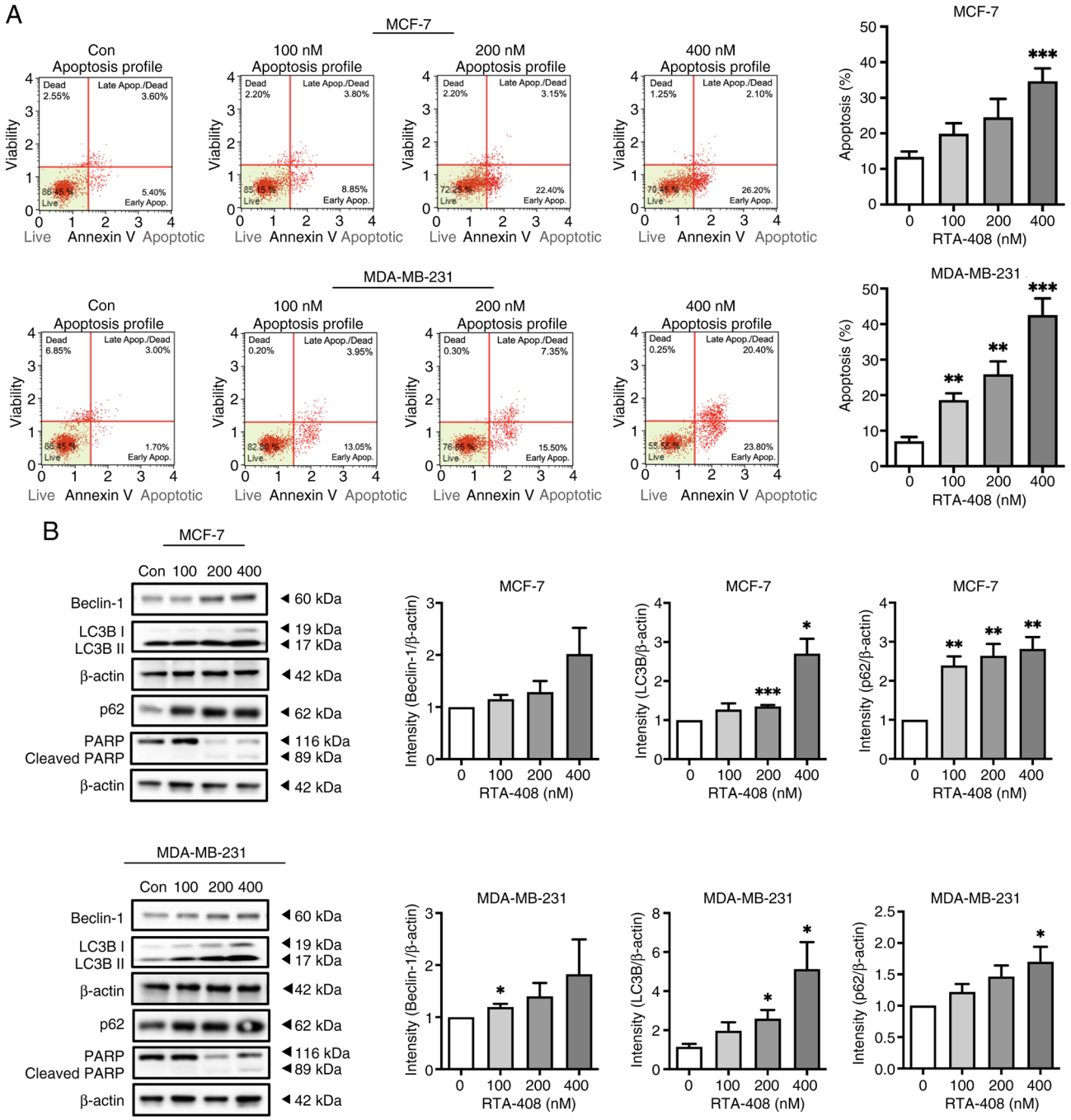

Figure 2. RTA-408 induces apoptosis and increases autophagy-associated marker accumulation in breast cancer cells. (A) Representative Annexin V & Dead Cell Kit flow cytometry dot plots of MCF-7 and MDA-MB-231 cells following 72-h exposure to vehicle Con or RTA-408 at 100, 200 or 400 nM. Quadrants denote live, early apoptotic, late apoptotic/dead and dead populations. Bar graphs to the right summarize total apoptosis (early + late apoptotic populations) as a percentage of total events. Data are presented as the mean ± SD (n=6). (B) Representative western blots of Beclin-1, LC3B-I/LC3B-II, p62, PARP and β-actin in MCF-7 and MDA-MB-231 cells after 72 h treatment with the indicated concentrations of RTA-408. Molecular weight markers are indicated. The PARP blot shows full-length PARP (116 kDa) and cleaved PARP (89 kDa). Right-side bar graphs show densitometric quantification of beclin-1, LC3B-IIand p62 normalized to β-actin and expressed relative to the control group. Data are presented as the mean ± SD (n=6). Statistical significance was determined by one-way ANOVA, followed by Tukey's post hoc test: *P<0.05, **P<0.01 and ***P<0.001 vs. control. Con, control; Apop., apoptosis; LC3B, microtubule-associated protein 1 light chain 3B; PARP, poly (ADP-ribose) polymerase.

phosphorylation of JNK, p38 and ERK were quantified after 72 h of exposure to 0-400 nM. In MCF-7 cells, p-JNK increased by ~2-fold at 100 nM and ~6-fold at 400 nM, whereas total JNK remained unchanged, indicating robust pathway activation (Fig. 3). p-p38 exhibited a modest yet significant increase at 400 nM and p-ERK displayed a significant 3-fold increase at the highest dose, determining the concurrent engagement of multiple MAPK branches without altering the total p38 or ERK abundance (Fig. 3). In MCF-7 cells, p-JNK was significantly increased at 100 and 200 nM (both P<0.05) and at 400 nM (P<0.01), p-p38 was significantly increased at 200 nM (P<0.001) and 400 nM (P<0.05), whereas p-ERK reached statistical significance only at 400 nM (P<0.05). In MDA-MB-231 cells, p-JNK

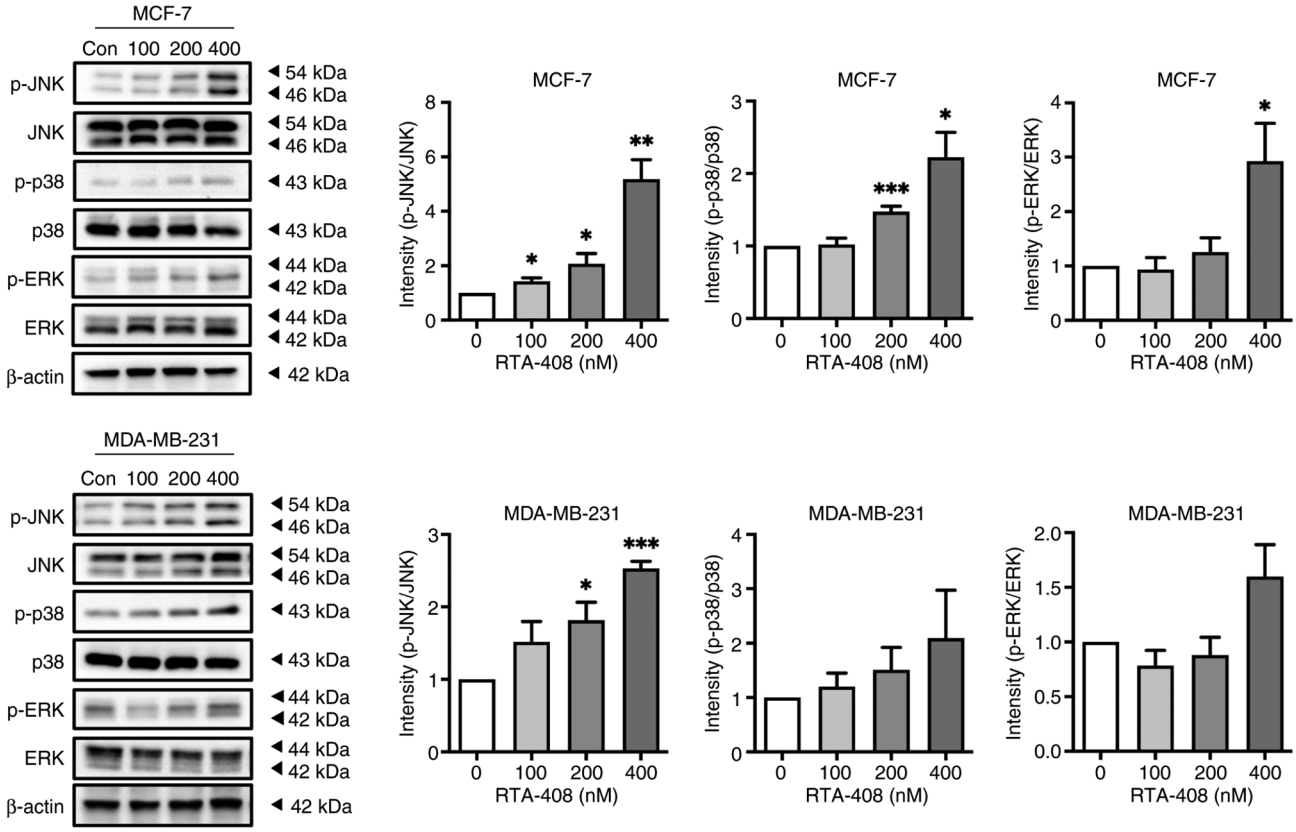

Figure 3. RTA-408 activates MAPK signaling in breast cancer cells. MCF-7 and MDA-MB-231 cells were treated with vehicle (Con) or RTA-408 at 100, 200 or 400 nM for 72 h. Western blotting was used to quantify whole-cell lysates for p- and total JNK, p38 and ERK; β-actin served as the loading control. Representative western blots are shown (left). Bar graphs (right) depict densitometric ratios of p- to total kinase (p-JNK/JNK, p-p38/p38 and p-ERK/ERK), normalized to the vehicle control (set to 1.0). RTA-408 elicited a concentration-dependent increase in p-JNK in both cell lines, with additional increases in p-ERK at the highest concentration and modest elevations of p-p38 (particularly in MCF-7). Data are presented as the mean ± SD (n=6). Statistical significance was determined by one-way ANOVA with Tukey's post-hoc test: *P<0.05, **P<0.01 and ***P<0.001 vs. control. p-, phosphorylated; Con, control.

reached statistical significance at 200 nM (P<0.05) and 400 nM (P<0.001), whereas p-p38 and p-ERK did not reach statistical significance at the tested concentrations. These findings demonstrate dose-dependent stimulation of JNK and ERK and, to a lesser extent, p38 signaling cascades by RTA-408, implicating MAPK activation in its downstream cytotoxic mechanisms (Fig. 3).

JNK inhibitor SP600125 inhibits RTA-408-induced JNK phosphorylation in BC cells. To build upon the JNK phosphorylation demonstrated in Fig. 3, the pharmacologic JNK inhibitor SP600125 was used as an initial tool to probe JNK pathway involvement. To determine whether JNK activation was a direct downstream target of RTA-408, both BC cell lines were treated with RTA-408 alone or in combination with SP600125 and the ratio of phosphorylated to total JNK was quantified. In MCF-7 cells, RTA-408 alone exhibited an ~3.5-fold increase in p-JNK relative to the control (P<0.001), whereas co-treatment with SP600125 reduced this increase to ~1.5-fold (P<0.01 vs. RTA-408 alone). An analogous pattern was observed in MDA-MB-231 cells; RTA-408 increased p-JNK by ~3-fold (P<0.01) and inhibition with SP600125 reduced phosphorylation to baseline. Total JNK and β-actin remained unchanged, indicating that RTA-408 increased JNK phosphorylation and that this effect was attenuated by pharmacologic inhibition (Fig. 4).

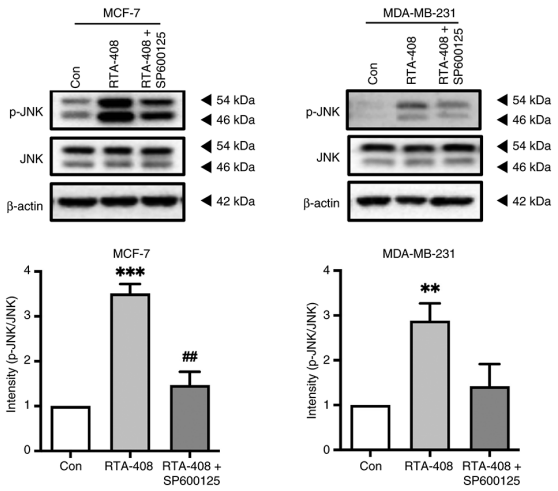

Figure 4. Pharmacologic JNK inhibition attenuates RTA-408-induced JNK phosphorylation. MCF-7 and MDA-MB-231 cells were treated with vehicle (Con), RTA-408 (400 nM; 72 h) or RTA-408 in the presence of the pharmacologic JNK inhibitor SP600125 (10 μM; 1 h pretreatment followed by co-incubation). Western blotting was used to quantify whole-cell lysates for p-JNK and total JNK; β-actin served as the loading control. Representative blots are shown. Bar graphs depict densitometric ratios of p-JNK to total JNK, normalized to vehicle (set to 1.0). RTA-408 markedly increased p-JNK in both cell lines, whereas SP600125 significantly reduced this elevation. Data are presented as the mean ± SD (n=6). Statistical analysis used one-way ANOVA with Tukey's post-hoc test: **P<0.01 and ***P<0.001 vs. control; $^{\#\#}$P<0.01 vs. RTA-408 alone. Con, control; p-, phosphorylated.

JNK inhibitor SP600125 inhibits RTA-408-induced apoptosis and autophagy in BC cells. To evaluate whether JNK signaling contributes to the RTA-408-induced phenotype, cells were treated with RTA-408 in the absence or presence of the pharmacologic JNK inhibitor SP600125. Annexin V & Dead Cell Kit flow cytometric analysis showed that RTA-408 significantly increased total apoptosis in both MCF-7 and MDA-MB-231 cells (Fig. 5A). Co-treatment with SP600125 reduced the apoptotic fraction in both cell lines; however, in MCF-7 cells, this decrease represented only a downward trend and did not reach statistical significance, whereas in MDA-MB-231 cells, the attenuation was statistically significant (Fig. 5A).

To further support apoptosis biochemically, PARP cleavage was examined by western blotting. RTA-408 increased cleaved PARP, and this effect was reduced in the presence of SP600125, consistent with the flow cytometric findings (Fig. 5B). Western blotting analysis further showed that RTA-408 increased beclin-1, LC3B-II and p62 in both cell lines and these changes were attenuated by SP600125 (Fig. 5B). In MCF-7 cells, SP600125 treatment significantly reduced the RTA-408-induced increases in beclin-1, LC3B-II and p62. In MDA-MB-231 cells, SP600125 treatment significantly reduced LC3B-II and p62, whereas beclin-1 showed a decreasing trend without statistical significance. Collectively, these findings support that JNK signaling contributes, at least in part, to RTA-408-induced apoptosis, and that the accumulation of autophagy-related markers was attenuated, at least in part, by pharmacologic JNK inhibition.

Discussion

RTA-408 is a synthetic triterpenoid antioxidant and inflammatory modulator with broad antitumor activity (19). Probst *et al* (19) first reported that RTA-408 inhibited the growth of numerous human tumor cells at nanomolar concentrations, including eight tumor cell lines: Melanoma, non-small cell lung cancer, breast adenocarcinoma, colorectal cancer, renal cancer and pancreatic cancer. In these cells, RTA-408 notably induced caspase activation and substrate cleavage, demonstrating a pro-apoptotic effect. Previous studies have explored the broad antitumor potential of RTA-408 (19). For example, in a drug-resistant lung cancer model, RTA-408 effectively overcame cisplatin resistance by downregulating WW domain-containing E3 ubiquitin-protein ligase 1, thereby blocking the ubiquitination and degradation of nuclear receptor coactivator 4 and inducing ferritinophagy and ferroptosis, demonstrating that RTA-408 may reverse chemotherapy resistance in lung cancer (20). Similarly, in the context of malignant brain tumors, RTA-408 demonstrated potent inhibitory effects against advanced/drug-resistant glioblastoma multiforme cells, effectively inhibiting the proliferation and colony formation of temozolomide-resistant glioblastoma cells and inducing G_1 cell cycle arrest and dose-dependent apoptosis (21). These findings highlight the broad-spectrum inhibitory efficacy of RTA-408 across a number of cancer cell types and states and its potential for clinical application. To the best of our knowledge, the present study provides the first detailed mechanistic characterization of RTA-408 in both ER-positive/hormone receptor-positive and triple-negative BC cell models, demonstrating nanomolar, dose-dependent antiproliferative effects together with apoptosis-associated responses, autophagy-related marker accumulation and JNK pathway involvement. These findings build on a previous report showing that RTA-408 inhibited tumor-cell growth and induced caspase activity/apoptosis in a broad human tumor-cell panel, including melanoma, non-small cell lung cancer, breast adenocarcinoma, colorectal carcinoma, renal cell adenocarcinoma and pancreatic cancer (19). Its antitumor activity has also been extended to resistant tumor settings, including cisplatin-resistant lung cancer and temozolomide-resistant glioblastoma, through mechanisms involving ferritinophagy/ferroptosis, apoptosis and cell-cycle arrest, as well as to glioblastoma models through CDC20 downregulation (20-22). Furthermore, the first-in-human phase I evaluation of oral omaveloxolone in patients with stage IV relapsed/refractory melanoma or non-small cell lung cancer, together with recent evidence of JNK-mediated antitumor and radiosensitizing activity in glioblastoma models, supports its broader translational relevance (15,23).

In the present study, a significant increase was observed in the expression of both apoptosis- and autophagy-associated markers in BC cells after RTA-408 treatment. For example, the number of cells positive for Annexin V/7-amino-actinomycin D (7-AAD) double staining increased, along with elevated expression of the autophagy-associated proteins Beclin-1, LC3B-II and p62. It should also be noted that although Annexin V/7-AAD-based flow cytometry demonstrated a clear dose-dependent increase in apoptotic cells, the cleaved PARP signal was relatively weak in the western blot analysis. This discrepancy may reflect differences in assay sensitivity or the timing of PARP cleavage detection. Therefore, PARP cleavage was considered supportive biochemical evidence, whereas Annexin V/7-AAD-based flow cytometry was used as the primary quantitative readout of apoptosis in the present study. This phenomenon of concurrent apoptosis and autophagy-associated marker accumulation has also been reported in other studies. For example, the small-molecule compound 1,3-dibutyl-2-thiooxo-imidazolidine-4,5-dione (C1) was shown to induce non-canonical autophagy and apoptosis in multiple human cancer cell lines through ROS-dependent ERK and JNK activation, while curcumin induced both apoptosis and autophagy in osteosarcoma MG63 cells (22,23). However, the functional role of autophagy in determining cell fate remains unclear. Autophagy may serve as a cellular stress defense response, promoting cell survival and delaying apoptosis, however, under specific circumstances, autophagy can also serve as a specialized pathway that promotes cell death (24). For example, a previous study showed that complete inhibition of autophagy with 3-methyladenine markedly enhanced curcumin-induced apoptosis in osteosarcoma cells, suggesting that autophagy serves a protective role under these conditions, potentially counteracting apoptosis (25). Therefore, it is currently hypothesized that autophagy may serve either a pro-death or a companion (protective) role in different contexts, with complex cross-regulation between autophagy and apoptotic signaling (26). The concurrent increase in apoptosis and autophagy-associated markers detected in the present study

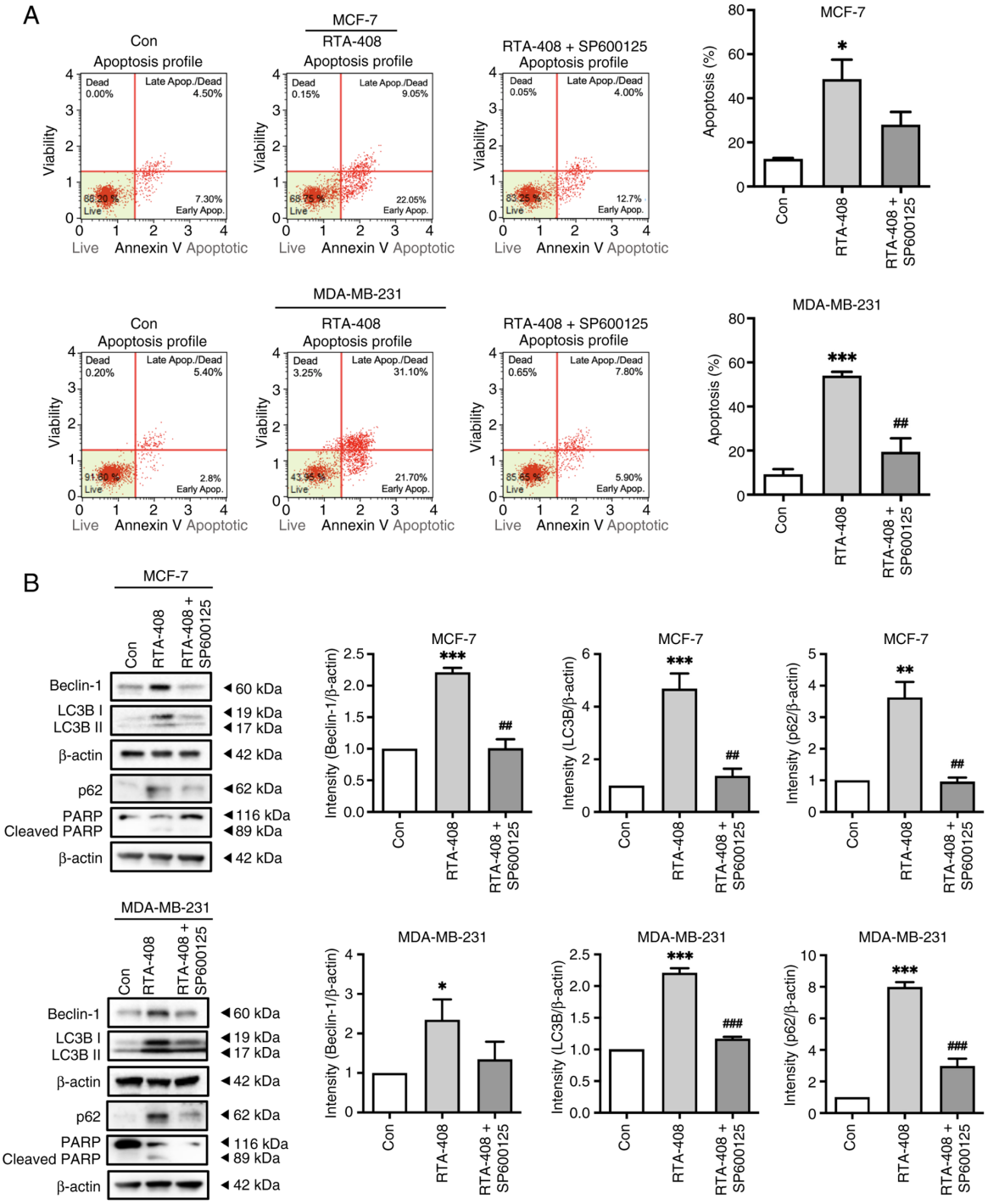

Figure 5. Pharmacologic JNK inhibition attenuates RTA-408-induced apoptosis and autophagy-associated marker accumulation. (A) Representative Annexin V & Dead Cell Kit flow cytometry plots of MCF-7 and MDA-MB-231 cells after 72 h treatment with vehicle control (Con), RTA-408 (400 nM) or RTA-408 + SP600125 (10 μM; 1 h pretreatment followed by co-treatment). Bar graphs to the right summarize total apoptosis (early + late apoptotic populations) as a percentage of total events. RTA-408 significantly increased apoptotic fractions in both cell lines. SP600125 reduced RTA-408-induced apoptosis in both cell lines; this reduction did not reach statistical significance in MCF-7 cells but was significant in MDA-MB-231 cells. (B) Representative western blots of beclin-1, LC3B-I/LC3B-II, p62, PARP and β-actin in MCF-7 and MDA-MB-231 cells under the same treatment conditions. Molecular weight markers are indicated. The PARP blot shows full-length PARP (116 kDa) and cleaved PARP (89 kDa). Right-side histograms show densitometric quantification of beclin-1, LC3B-II and p62 normalized to β-actin and expressed relative to the control group. SP600125 attenuated the RTA-408-induced increases in beclin-1, LC3B-II and p62 in MCF-7 cells and reduced LC3B-II and p62 accumulation in MDA-MB-231 cells, with a decreasing trend in beclin-1. Data are presented as the mean ± SD (n=6). Statistical significance was determined by one-way ANOVA followed by Tukey's post hoc test: *P<0.05, **P<0.01 and ***P<0.001 vs. control; $^{\#\#}$P<0.01 and $^{\#\#\#}$P<0.001 vs. RTA-408 alone. Con, control; Apop., apoptosis; LC3B, microtubule-associated protein 1 light chain 3B; PARP, poly (ADP-ribose) polymerase.

suggests that RTA-408 induces apoptosis and is associated with the accumulation of these markers. However, because autophagic flux was not directly assessed using lysosomal inhibitors, these findings do not distinguish between enhanced autophagosome formation from impaired autophagosome degradation.

In the present study, phosphorylation of JNK, p38 and ERK was assessed at a single 72 h endpoint after RTA-408

treatment. At this measured time point, JNK showed the largest increase in phosphorylation among the MAPK pathways examined, whereas p38 changes were more modest and ERK phosphorylation was increased mainly at the highest concentration. These findings support the involvement of MAPK signaling, particularly JNK, in the cellular response to RTA-408. However, because no time-course analysis was performed, the activation kinetics of these pathways cannot be determined from the present data.

To determine that the aforementioned cell death effects were indeed dependent on JNK signaling, the pharmacologic inhibitor SP600125 was used to block JNK activity. The results showed that the addition of SP600125 significantly reversed RTA-408-induced apoptosis and autophagy. Specifically, treatment with SP600125 reduced annexin V positivity and PARP cleavage while also inhibiting or abolishing the increase in autophagy markers LC3B-II and beclin-1, demonstrating that both RTA-408-induced apoptosis and autophagy are JNK-dependent (25). Similar evidence has been previously reported. For example, the JNK-specific inhibitor SP600125 effectively blocked curcumin-induced autophagy in osteosarcoma cells, demonstrating that the JNK pathway serves a key role in curcumin-induced autophagy (23). Furthermore, SP600125 has been shown to simultaneously inhibit resveratrol-induced autophagy and apoptosis, further supporting the idea that JNK is a common upstream regulator of both cell death processes (27). These results validate the mechanism proposed in the present study: RTA-408 simultaneously activates intracellular apoptosis and autophagy by triggering the JNK pathway.

Previous research regarding RTA-408 and associated triterpenoidderivatives(suchas2-cyano-3,12-dioxooleana-1,9-dien-28-oic acid) has primarily focused on the Nrf2 antioxidant and NF-κB anti-inflammatory pathways (19). As an antioxidant-inflammatory modulator, RTA-408 binds to KEAP1 and stabilizes Nrf2 at low concentrations, inducing the expression of downstream antioxidant genes [such as NAD(P)H quinone dehydrogenase 1 (NQO1) and heme oxygenase 1 (HO-1)], while inhibiting the expression of pro-inflammatory mediators, including nitric oxide synthase 2, prostaglandin-endoperoxide synthase 2, C-C motif chemokine ligand 2 and C-C motif chemokine ligand 5 (19). By increasing Nrf2 activity, RTA-408 can reduce oxidative stress and inflammation in the tumor microenvironment, thereby reversing tumor-induced immune evasion and inhibiting tumor growth and metastasis (19). Previous studies have shown that RTA-408 modulates several oncogenic signaling pathways at antiproliferative concentrations. In a broad human tumor-cell panel, RTA-408 inhibited NF-κB signaling in a manner consistent with IKKβ inhibition, decreased cyclin D1 levels, increased CDKN1A/p21 expression and enhanced JNK phosphorylation at concentrations that inhibited tumor-cell growth and induced caspase activity/apoptosis (19). More recent studies further reported that RTA-408/omaveloxolone induced G1 cell-cycle arrest, apoptosis and caspase-3 activation in temozolomide-resistant glioblastoma cells as well as suppressed glioblastoma growth *in vitro* and *in vivo* through cell-cycle arrest associated with CDC20 downregulation (21,22). In addition, JNK inhibition has been shown to reverse RTA-408-mediated reductions in cell viability, apoptosis induction, migration inhibition and radiosensitization in glioblastoma models, supporting functional involvement of JNK signaling in another cancer context (23).

The novelty of the present study lies in extending the mechanistic understanding of RTA-408 in BC cells beyond its previously described Nrf2-centered antioxidant/anti-inflammatory functions and antitumor effects in other cancer models (15,19-23). The present findings show that, in ER-positive/hormone receptor-positive and triple-negative BC cell models, RTA-408 increases JNK phosphorylation and is associated with annexin V-defined apoptosis, PARP cleavage and accumulation of autophagy-related markers. These results suggest that MAPK-JNK-associated pro-death signaling contributes to the cellular response to RTA-408 in BC cells and may provide a basis for further evaluating this compound in BC. However, since Nrf2 activity and autophagic flux were not directly assessed, the relationship among oxidative-stress modulation, JNK activation and autophagy-associated marker accumulation remains to be clarified. Despite this, a number of limitations in the present study should be acknowledged. First, the present study was conducted exclusively *in vitro* using two-dimensional monolayer cultures, which did not recapitulate the tumor microenvironment, stromal and immune interactions or the pharmacokinetic and metabolic constraints present *in vivo*; therefore, the efficacy and safety of RTA-408 cannot be directly extrapolated to the clinical setting. Second, although SP600125 attenuated the effects of RTA-408, JNK involvement was evaluated solely with this pharmacologic inhibitor. In the absence of genetic approaches, such as siRNA/shRNA-mediated knockdown or dominant-negative JNK constructs, definitive mechanistic specificity cannot be established and off-target effects remain possible. Third, Nrf2 signaling was not directly assessed in the present study, as nuclear Nrf2 accumulation and canonical downstream targets such as NQO1 and HO-1 were not measured. Consequently, the association between Nrf2 activation and JNK signaling could be determined from the present dataset, and the possibility that RTA-408 exerts dose-dependent cytoprotective and cytotoxic effects through distinct pathways remains to be clarified. In addition, although RTA-408 increased beclin-1, LC3B-II and p62 accumulation, autophagic flux was not directly assessed using lysosomal inhibitors; therefore, the present data cannot distinguish between increased autophagosome formation and impaired autophagosome degradation. Fourth, non-malignant mammary epithelial cells were not included; thus, tumor selectivity and safety could not be inferred from the present study. In addition, the development of drug resistance, the reversibility of growth inhibition after prolonged exposure or the potential interaction of RTA-408 with standard chemotherapeutic, endocrine or HER2-targeted therapies were not evaluated. These issues represent important gaps that warrant further mechanistic, translational and *in vivo* investigation.

In conclusion, the present study found that RTA-408 exerted dose-dependent antiproliferative effects in both MCF-7 and MDA-MB-231 BC cells. RTA-408 increased

annexin V-defined apoptosis, PARP cleavage and JNK phosphorylation, and was accompanied by the accumulation of the autophagy-associated markers beclin-1, LC3B-II and p62. Pharmacologic inhibition with SP600125 attenuated JNK phosphorylation, reduced apoptotic responses and diminished autophagy-related marker accumulation, supporting that JNK signaling contributes, at least in part, to these effects. Given the lack of direct autophagic flux analysis, genetic validation of JNK and inclusion of normal mammary epithelial cell controls, these findings should be interpreted cautiously and support further mechanistic and *in vivo* evaluation of RTA-408 in BC models.

Acknowledgements

Not applicable.

Funding

The present study was supported by grants from An-Nan Hospital, China Medical University, Taiwan (grant nos. ANHRF114-17 and ANHRF114-27).

Availability of data and materials

The datasets generated in the present study may be requested from the corresponding author.

Authors' contributions

YJC and HPT conceived and designed the present study. YJC performed the majority of the experiments and collected the data. MYC, IHC, WCC, TTT and CYW assisted with data acquisition and interpretation. HPT and JHL supervised the research and analyzed the data. HPT and JHL confirm the authenticity of all the raw data. YJC and HPT drafted the manuscript. JHL critically revised the manuscript for important intellectual content. All authors read and approved the final version of the manuscript.

Ethics approval and consent to participate

Not applicable.

Patient consent for publication

Not applicable.

Competing interests

The authors declare that they have no competing interests.

Use of artificial intelligence tools

During the preparation of this work, artificial intelligence tools were used to improve the readability and language of the manuscript or to generate images, and subsequently, the authors revised and edited the content produced by the artificial intelligence tools as necessary, taking full responsibility for the ultimate content of the present manuscript.

References

1. Bray F, Laversanne M, Sung H, Ferlay J, Siegel RL, Soerjomataram I and Jemal A: Global cancer statistics 2022: GLOBOCAN estimates of incidence and mortality worldwide for 36 cancers in 185 countries. CA Cancer J Clin 74: 229-263, 2024.
2. Arnold M, Morgan E, Rumgay H, Mafra A, Singh D, Laversanne M, Vignat J, Gralow JR, Cardoso F, Siesling S and Soerjomataram I: Current and future burden of breast cancer: Global statistics for 2020 and 2040. Breast 66: 15-23, 2022.
3. Cao W, Chen HD, Yu YW, Li N and Chen WQ: Changing profiles of cancer burden worldwide and in China: A secondary analysis of the global cancer statistics 2020. Chin Med J (Engl) 134: 783-791, 2021.
4. Osborne CK and Schiff R: Mechanisms of endocrine resistance in breast cancer. Annu Rev Med 62: 233-247, 2011.
5. Grann VR, Troxel AB, Zojwalla NJ, Jacobson JS, Hershman D and Neugut AI: Hormone receptor status and survival in a population-based cohort of patients with breast carcinoma. Cancer 103: 2241-2251, 2005.
6. Early Breast Cancer Trialists' Collaborative Group (EBCTCG), Davies C, Godwin J, Gray R, Clarke M, Cutter D, Darby S, McGale P, Pan HC, Taylor C, *et al*: Relevance of breast cancer hormone receptors and other factors to the efficacy of adjuvant tamoxifen: patient-level meta-analysis of randomised trials. Lancet 378: 771-784, 2011.
7. Daly B, Olopade OI, Hou N, Yao K, Winchester DJ and Huo D: Evaluation of the quality of adjuvant endocrine therapy delivery for breast cancer care in the United States. JAMA Oncol 3: 928-935, 2017.
8. Roberts K, Rickett K, Greer R and Woodward N: Management of aromatase inhibitor induced musculoskeletal symptoms in postmenopausal early breast cancer: A systematic review and meta-analysis. Crit Rev Oncol Hematol 111: 66-80, 2017.
9. Tamirisa N and Hunt KK: Neoadjuvant chemotherapy, endocrine therapy, and targeted therapy for breast cancer: ASCO guideline. Ann Surg Oncol 29: 1489-1492, 2022.
10. Chan CWH, Tai D, Kwong S, Chow KM, Chan DNS and Law BMH: The effects of pharmacological and non-pharmacological interventions on symptom management and quality of life among breast cancer survivors undergoing adjuvant endocrine therapy: A systematic review. Int J Environ Res Public Health 17: 2950, 2020.
11. Ross JS, Fletcher JA, Linette GP, Stec J, Clark E, Ayers M, Symmans WF, Pusztai L and Bloom KJ: The Her-2/neu gene and protein in breast cancer 2003: Biomarker and target of therapy. Oncologist 8: 307-325, 2003.
12. Piccart-Gebhart MJ, Procter M, Leyland-Jones B, Goldhirsch A, Untch M, Smith I, Gianni L, Baselga J, Bell R, Jackisch C, *et al*: Trastuzumab after adjuvant chemotherapy in HER2-positive breast cancer. N Engl J Med 353: 1659-1672, 2005.
13. Lower EE, Glass E, Blau R and Harman S: HER-2/neu expression in primary and metastatic breast cancer. Breast Cancer Res Treat 113: 301-306, 2009.
14. Slamon D, Eiermann W, Robert N, Pienkowski T, Martin M, Press M, Mackey J, Glaspy J, Chan A, Pawlicki M, *et al*: Adjuvant trastuzumab in HER2-positive breast cancer. N Engl J Med 365: 1273-1283, 2011.
15. Creelan BC, Gabrilovich DI, Gray JE, Williams CC, Tanvetyanon T, Haura EB, Weber JS, Gibney GT, Markowitz J, Proksch JW, *et al*: Safety, pharmacokinetics, and pharmacodynamics of oral omaveloxolone (RTA 408), a synthetic triterpenoid, in a first-in-human trial of patients with advanced solid tumors. Onco Targets Ther 10: 4239-4250, 2017.
16. Wu Y, Zhang Y, Ge L, He S, Zhang Y, Chen D, Nie Y, Zhu M and Pang Q: RTA408 alleviates lipopolysaccharide-induced acute lung injury via inhibiting Bach1-mediated ferroptosis. Int Immunopharmacol 142: 113250, 2024.
17. Lynch DR, Chin MP, Delatycki MB, Subramony SH, Corti M, Hoyle JC, Boesch S, Nachbauer W, Mariotti C, Mathews KD, *et al*: Safety and efficacy of omaveloxolone in friedreich ataxia (MOXIe Study). Ann Neurol 89: 212-225, 2021.
18. Dasgupta D, Tripathi A, Griffard-Smith R, Yellapu N, Dhorajiya P and Pyaram K: Therapeutic potential of NRF2 activating drug RTA-408 in suppressing T cell effector responses and inflammatory bowel disease. J Immunol 214: 1951-1968, 2025.
19. Probst BL, Trevino I, McCauley L, Bumeister R, Dulubova I, Wigley WC and Ferguson DA: RTA 408, a novel synthetic triterpenoid with broad anticancer and anti-inflammatory activity. PLoS One 10: e0122942, 2015.

20. Wang X, Liu T, Fei Y, Zhang S, Yang Y, Chen Z, Zhu R, Deng S, Zhang T, Wu D and Xu Y: RTA-408 overcomes cisplatin-resistant lung cancer by inhibiting WWP1-mediated NCOA4 ubiquitination to induce ferritinophagy and ferroptosis. Free Radic Biol Med 238: 595-610, 2025.
21. Lee KT, Lieu AS, Lin CL, Hsu YC and Tsai TH: Synthetic oleanolic acid derivative, RTA-408, overcome in TMZ-resistant glioblastoma cells by inducing apoptosis and G1 cell cycle arrest. Med Oncol 42: 353, 2025.
22. Lee KT, Hsu YC, Lieu AS, Lin CL and Tsai TH: Omaveloxolone suppresses cell growth and causes cell cycle arrest by downregulating CDC20 expression in glioblastoma cells both in vitro and in vivo. J Cell Mol Med 29: e70607, 2025.
23. Tsai HP, Qin H, Chong YB, Chen IH, Kuo SH, Tseng TT and Lieu AS: RTA-408 enhances radiosensitivity and inhibited tumor progression via JNK pathway in glioblastoma. Kaohsiung J Med Sci: e70142, 2025 (Epub ahead of print).
24. Wong CH, Iskandar KB, Yadav SK, Hirpara JL, Loh T and Pervaiz S: Simultaneous induction of non-canonical autophagy and apoptosis in cancer cells by ROS-dependent ERK and JNK activation. PLoS One 5: e9996, 2010.
25. Zhang Y, Chen P, Hong H, Wang L, Zhou Y and Lang Y: JNK pathway mediates curcumin-induced apoptosis and autophagy in osteosarcoma MG63 cells. Exp Ther Med 14: 593-599, 2017.
26. Eisenberg-Lerner A, Bialik S, Simon HU and Kimchi A: Life and death partners: Apoptosis, autophagy and the cross-talk between them. Cell Death Differ 16: 966-975, 2009.
27. Zhang J, Ping J, Jiang N and Xu L: Resveratrol inhibits hepatic stellate cell activation by regulating autophagy and apoptosis through the SIRT1 and JNK signaling pathways. J Food Biochem 46: e14463, 2022.